Acta Cryst. (1978). A**34**, 362–367

Pendellösung Effects as a Tool for Examining Minute Strains with a Triple-Crystal X-ray Spectrometer

BY OLE ALSTRUP

Laboratory of Applied Physics III, *Building* 307, *Technical University of Denmark, DK*-2800 *Lyngby, Denmark*

(*Received* 4 *October* 1977; *accepted* 7 *November* 1977)

Plane-wave *Pendellösung* effects are shown to be effective and very sensitive for analyzing minute strains in silicon crystals with dimensions normally used for practical applications. In a triple-crystal silicon X-ray spectrometer with an angular beam divergence of less than 0·1″ the *Pendellösung* effect is very pronounced for sample thicknesses up to 1·2 mm. Strain fields are shown for silicon crystals implanted with 60 keV phosphorus ions for doses down to 10^{13} ion cm^{-2} and the limit of resolution is one order of magnitude less.

Introduction

The *Pendellösung* effect which refers to the interference between two coherent wave fields in a crystal was first observed for X-rays by Kato & Lang (1959) in the transmission case. In most of the succeeding papers concerning this *Pendellösung* effect the topographical picture of *Pendellösung* fringes is due to the spherical properties of the X-ray wave field. As shown by Kato (1961) a spherical wave excites such a great portion of the dispersion surfaces, that wave fields from the α and β branches having parallel Poynting vectors are created simultaneously (*e.g.* points A and A' in Fig. 1). Beating of these waves will produce topographical *Pendellösung* fringes in the transmission case for wedge-shaped crystals.

If a highly collimated X-ray beam is used, the wave field becomes almost planar, and only a small region of the dispersion surfaces will be excited (around A and B in Fig. 1). Although the Poynting vectors have different directions these two fields may interfere over a considerable volume if the beam is not too narrowly defined by collimator slits. This constitutes the plane-wave interference effect as predicted by Ewald. It has later been verified by several authors, as intensity variations in the rocking curve from thin crystals and as topographical fringes in wedge-shaped crystals by Malgrange & Authier (1965), Kohra & Kikuta (1968) and Lefeld-Sosnowska & Malgrange (1968).

In the present paper it is shown that when a crystal collimated beam with sufficiently small angular divergence is used together with a critical adjustment of the sample crystal the *Pendellösung* effect may become so significant that both intensity variations and fringes are observable in crystals of normal thickness and with plane parallel surfaces. As the fringe pattern is very sensitive to strains the method described may become useful for analysing strains in otherwise perfect crystals.

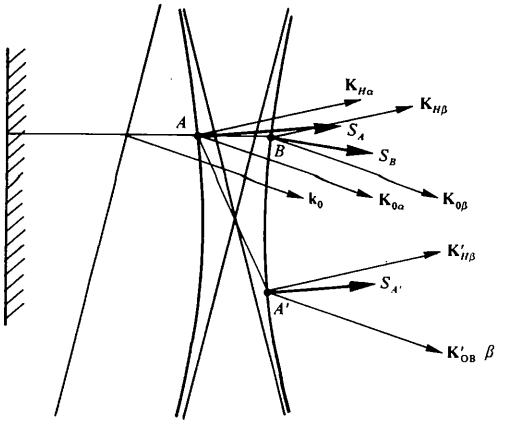

Fig. 1. Dispersion surface for one polarization state. The wave fields from tiepoints A and A' will interfere for spherical waves, and those from A and B for plane waves.

Experimental technique

The principle of the experimental set-up is shown in Fig. 2. The X-ray beam is collimated in two asymmetrically cut silicon crystals, *C*I and *C*II. All of the experiments have been carried out with Mo $K\alpha_1$ radiation from a 1 kW X-ray tube with point focus of 0·4 × 0·4 mm, and only 220 reflections have been investigated. Each collimator has an asymmetry factor $b = 0{\cdot}1$ ($b = \sin\varphi_1/\sin\varphi_2$, where φ_1 and φ_2 are the angles of incidence of the incoming and diffracted beams respectively). The divergence of the beam is 0·07″. The collimators are adjusted such that the $K\alpha_2$ beam does not intersect the reflecting surface of *C*II. In order to obtain *Pendellösung* fringe topographs no Soller slits were used for diminishing the vertical divergence of the beam. Hence the height of the beam is only limited by *C*II and the distance to the sample

crystal S. In most of the experiments the beam height was 20 mm and the width was 8 mm. Full beam size has also been used for measuring the rocking curves. The results indicate a high perfection of the crystal. The rocking curves were continuously recorded with a scintillation counter connected to an X–Y recorder; scanning through the rocking curve was by rotation of the sample goniometer by means of a piezoelectric crystal. The topographs were recorded on Kodak Industrex C films. Typical exposure times were 20 min.

All silicon crystals to be analysed were dislocation and swirl free. They were cut perpendicular to the $\langle 111 \rangle$ direction, so that symmetric Laue diffraction could be used. The crystals were subsequently etched or polished on both sides.

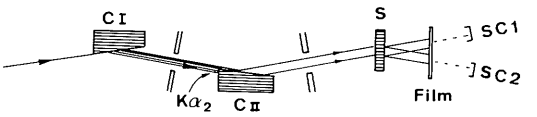

Fig. 2. Triple-crystal spectrometer. CI and CII are asymmetrically cut collimator crystals. CII is turned so that the $K\alpha_2$ beam does not hit the polished surface.

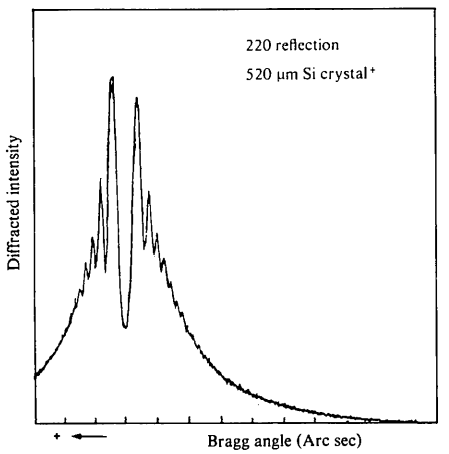

(*a*)

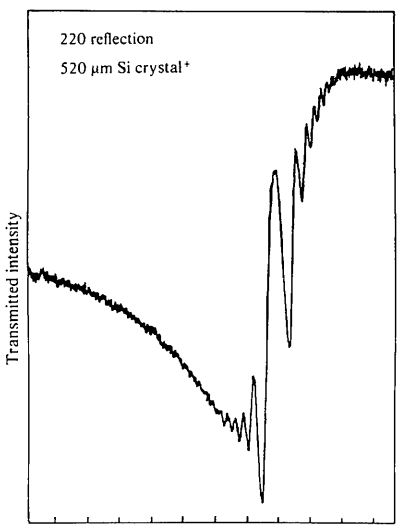

(*b*)

Fig. 3. Rocking curve for a 520 μm thick etched silicon crystal. 220 reflection for the Laue case. (*a*) Diffracted beam. (*b*) Transmitted beam.

Perfect crystals

Figs. 3 and 4 show examples of rocking curves for strain-free perfect crystals. Fig. 3(*a*) is characterized by a very large dip in the middle of the rocking curve, because most of the energy is transferred to the forward diffracted beam, which is shown in Fig. 3(*b*). A corresponding peak is seen here. In Fig. 4 the peaks are not so big, but the number is remarkable. Peaks are visible well outside the diffraction region normally considered.

The positions of the peaks are in good agreement with the dynamical theory of X-ray diffraction. In the formulae to be derived below the notation is rather close to the one used in the review article by Batterman & Cole (1964). The energy flow inside the crystal oscillates between the $\mathbf{K}_0$ and $\mathbf{K}_H$ directions as $\cos(2\pi Z/L)$, where Z is the depth in the crystal and $L = 1/(\mathbf{K}'_{0\alpha} - \mathbf{K}'_{0\beta})$ is the *Pendellösung* length. For L we get the equation

$$\frac{1}{L} = k|P|(1/\cos\theta)\,\Gamma F_H(\eta^2 + 1)^{1/2} = D_0(\eta^2 + 1)^{1/2},$$

where P is the polarization factor ($P = 1$ and $|\cos 2\theta|$ for the σ and π polarizations), $\Gamma = r_e . \lambda^2/\pi V$, where r_e is the classical electron radius and V is the volume of the unit cell. F_H is the structure factor for the hkl reflection

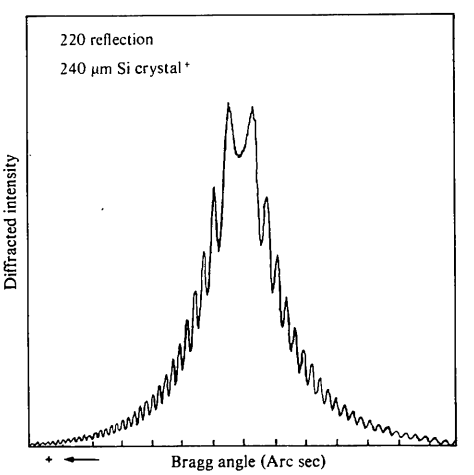

Fig. 4. Rocking curve for a 240 μm thick double polished silicon crystal (crystal *B*). 220 reflection for the Laue case, diffracted beam.

including the Debye–Waller factor, η is a normalized angle such that the half-maximum value of the rocking curve is obtained for $\eta = \pm 1$. For symmetric Laue diffraction $\eta = \Delta\theta \sin 2\theta/(\Gamma|P|F_H)$ where $\Delta\theta$ is the deviation from the exact Bragg angle. D_0 is the diameter of the dispersion hyperbola. For the 220 reflection in silicon we have $1/D_{0\sigma} = 36{\cdot}8$ μm and $1/D_{0\pi} = 39{\cdot}5$ μm for the σ and π polarizations.

The most pronounced *Pendellösung* effect for an unpolarized incident X-ray beam will be seen if the crystal has a thickness so that the difference between the number of *Pendellösung* lengths for the σ and π polarizations is an integer for $\eta = 0$. For the present experimental conditions this is obtained for crystal thicknesses $= N \times 550$ μm. This is in good agreement with the experiments. Fig. 3 shows the diffracted and transmitted rocking curves for a 520 μm thick crystal. The numbers of *Pendellösung* lengths Z/D are 14·1 and 13·2 for the σ and π polarizations respectively, so that the difference is close to one. For $\eta = 0$ we would expect most of the energy to be transferred to the transmitted beam as the Z/D values are so close to being integers. This is clearly seen to be the case.

In Fig. 4 the diffracted rocking curve is shown for a 240 μm thick crystal, hereafter called crystal *B*. Here the number of *Pendellösung* lengths for $\eta = 0$ are 6·5 and 6·1 respectively. Consequently the two polarized waves counteract each other for $\eta = 0$ and we would expect a minimal *Pendellösung* effect. Obviously the dip in the rocking curve for $\eta = 0$ is small as compared to that in Fig. 3, but even in this case the *Pendellösung* effect is considerable. In actual fact the effect will always be visible because a strict cancellation of the two fields will only take place for one specific η value. The peak intensity variation with crystal thicknesses agrees well with the results of Hart & Lang (1965).

In order to analyse further the interference pattern we look at the expression for the energy flow within the crystal. If we neglect absorption we have for one polarization state (Batterman & Cole, equation 50)

$$\mathbf{S}_T \simeq \tfrac{1}{2}a^2|E_0^i|^2(e^{-2\nu'}\mathbf{s}_0 + b\mathbf{s}_H) + \tfrac{1}{2}a^2|E_0^i|^2(e^{2\nu}\mathbf{s}_0 + b\mathbf{s}_H) + a^2|E_0^i|^2(\mathbf{s}_0 - b\mathbf{s}_H)\cos(2\pi ZD), \quad (1)$$

where $a = \frac{1}{2}\cosh^{-1}\nu$ and $\sinh\nu = \eta$. $\mathbf{s}_0$ and $\mathbf{s}_H$ are unit vectors in the $\mathbf{K}_0$ and $\mathbf{K}_H$ directions respectively, and E_0^i is the electric field of the incoming wave.

For the symmetric Laue case the intensity in the diffracted direction may thus be written

$$S_H \simeq a^2|E_0^i|^2(1 - \cos 2\pi ZD).$$

As the σ and π fields are perpendicular to each other we may simply add the intensities so that we get the following expression for the rocking curve

$$\frac{I}{I_0} \simeq \frac{1}{4(\eta^2+1)}\left[1 - \cos(2\pi\sqrt{\eta^2+1}\,D_{0\sigma}Z)\right] + \frac{1}{4(\eta'^2+1)}\left[1 - \cos(2\pi\sqrt{\eta'^2+1}\,D_{0\pi}Z)\right]. \quad (2)$$

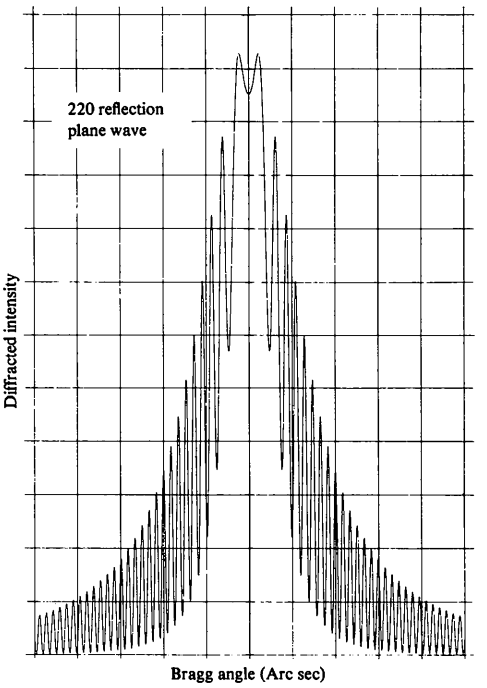

(*a*)

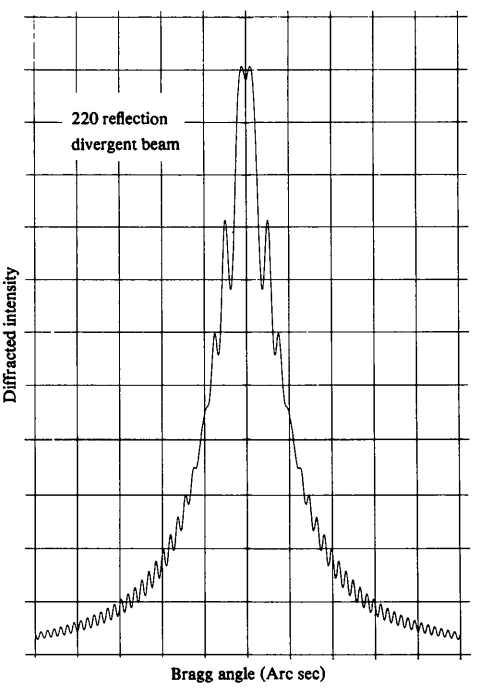

(*b*)

Fig. 5. Calculated rocking curve for crystal *B*. (*a*) Plane-wave approximation. (*b*) Angular divergence = 0·3″.

As we may write $\eta' = \eta/\cos 2\theta$ and $D_{0\pi} = D_{0\sigma} \cos 2\theta$ it is seen that for large η values the two intensity terms are always oscillating in phase. This may also be seen geometrically from Fig. 2 as the dispersion surfaces for both σ and π polarized waves approach the same asymptotes for large η values. On the other hand, the form of the rocking curve for small η values is very sensitive to the thickness of the crystal. Fig. 5 shows the rocking curve calculated for the data of crystal *B*. The agreement with Fig. 4 is well within the experimental error. The positions of the peaks for the two curves are shown in Table 1. For large η values the distance between the peaks approaches a constant which is 0·16 for the calculated curve and 0·18 for the experimental one. This difference is probably due to the difficulty in measuring the maximum and half-width values of Fig. 4. A reduction of the experimental values by 6% thus gives a much better agreement with calculation. The influence of crystal thickness is illustrated by the third column in Table 1. The peaks are here calculated for a 2% reduction of the *Z* value.

Table 1. *Position in η scale of experimental and calculated peaks in the rocking curve of crystal B*

Experimental	Theoretical	Theoretical (crystal thickness ×0·98)
0·30	0·22	0·30
0·64	0·61	0·65
0·90	0·87	0·90
1·11	1·08	1·12
1·31	1·28	1·32
1·50	1·47	1·51
1·70	1·65	1·69
1·87	1·82	1·87
2·05	2·00	2·05
2·22	2·16	2·22
2·40	2·33	2·38
2·59	2·50	2·55
2·74	2·66	2·72
2·92	2·82	2·89
3·11	2·98	3·05
3·29	3·14	3·21
3·46	3·30	3·38
3·62	3·46	3·54
3·82	3·62	3·70

In order to get an idea of how critical the beam collimation is, a simple calculation has been carried out where a part of the dispersion surface corresponding to a given angular divergence is assumed to be excited. The fields from 50 plane waves evenly distributed within this region have been summed. For an angular divergence of 0·07″ corresponding to the actual experimental case no change in the rocking curve was observed. With the divergence increased to 0·15″ practically the same number of peaks were visible but the peak height was approximately 30% smaller. Fig. 5(*b*) shows the rocking curve for an angular divergence of 0·30″. Here only the first few peaks will be visible above the background.

From equation (2) it is seen that a thicker crystal or a more uneven crystal surface is equivalent to an increased beam divergence. This is in agreement with Fig. 3, as this crystal was thicker and the surfaces were only etched whereas crystal *B* was polished optically flat on both sides. The calculated divergence dependence is also in agreement with another experiment where only one collimator crystal was used. The angular divergence was 0·7″ and no *Pendellösung* effect at all was observed.

Strain analysis

Because of the strong local intensity variations of the rocking curve the *Pendellösung* effect may be used as a tool for examining strains in crystals. If we use a perfect crystal with plane parallel surfaces as a sample and adjust it properly in the triple-crystal spectrometer so that the tilting angle β (β = the angle between the diffracting Bragg planes of the sample and the diffracting Bragg planes of the collimator crystals) is zero we will get a homogeneously exposed topograph, *i.e.* all parts of the crystal will be in the same condition of diffraction. However, if β differs from zero the Bragg condition is not fulfilled all over the sample but only in a horizontal band, the width of which depends on β (Renninger, 1963). Introducing the horizontal plane through the focus of the X-ray tube as our zero plane and considering a segment of the beam, we define φ as the angle of the beam with the horizontal plane. If the sample crystal exactly fulfills the Bragg condition in the zero plane, the deviation $\Delta\theta_\beta$ from the exact Bragg angle for other horizontal planes is given by

$$\Delta\theta_\beta \simeq \beta \sin \varphi. \qquad (3)$$

As sin φ is proportional to the height on the sample (or film) from the zero plane, we will depict the rocking curve on the film if $\beta \neq 0$. Fig. 6 shows examples of this for crystal *B*. β is approximately 0·8′ and 3′ respectively. The small curvature of the bands is probably due to bending or thickness variations of the crystal. The strain sensitivity of the topograph is inversely proportional to β. The typical distance between the peaks in Fig. 4 and thus between the fringes in Fig. 6 corresponds to a change in the Bragg angle of 0·25″. The broad band in the topographs corresponding to $\eta \simeq 0$ can be displaced vertically by turning the crystal through the Bragg angle so that full sensitivity may be obtained where desired. From equation (3) it is found that for the present experimental conditions (height of the beam = 20 mm and distance from X-ray tube = 500 mm) the *Pendellösung* peaks in Fig. 4 will disappear for β values greater than approximately 10″.

Some preliminary experiments have been carried out on ion-implanted samples with the aim of testing the applicability of the method. The samples were approxi-

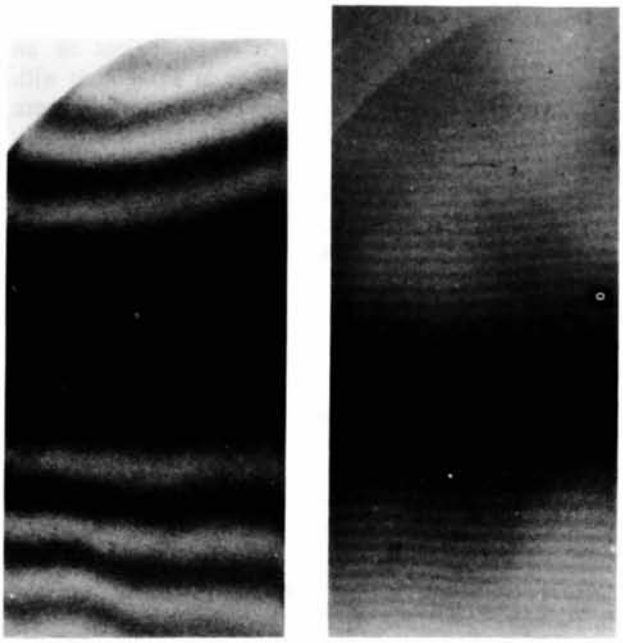

(*a*) (*b*)

Fig. 6. Transmission topography of crystal *B*. (*a*) Crystal tilted 0·8′. (*b*) Crystal tilted 3′.

mately 250 μm thick and polished on both surfaces, like crystal *B*. They were all implanted with 60 keV phosphorus ions at room temperature. In Fig. 7 are shown topographs of a sample implanted with 10^{13} ion cm^{-2} through a 10 × 10 mm hole with an arbitrary orientation of the edges. Outside the implanted area the fringe pattern consists of straight horizontal lines like the ones in Fig. 6, so the crystal is unstrained in this region (within the sensitivity of the method). Inside the implanted area the fringes are straight equidistant tilted lines, so that the strain field is homogeneous here. The horizontal distance between the fringes corresponds to the angular deviation as found from the rocking curve in Fig. 4. As the tilting angle β is decreased, the distance between the fringes increases and thus their slope will increase within the implanted region because their horizontal distance is unchanged. This effect is shown in Fig. 7(*c*), where β is diminished to approximately 1′. From this result it may be concluded that strain fields from implanted doses down to 10^{12} ion cm^{-2} for these low-energy ions may readily be observed. For $\beta = 0$ a slight change in intensity was observed within the implanted spot but no fringes were observed. With this dose the strain field is so small that the peaks are still significant in the rocking curve.

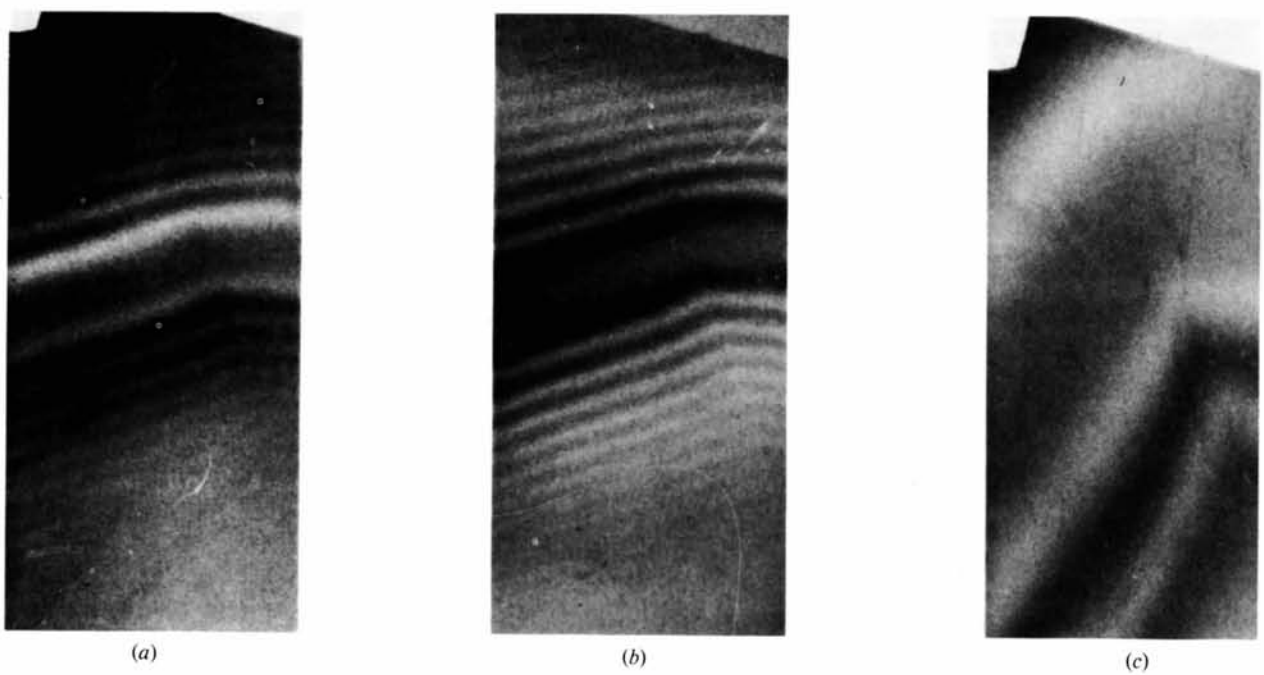

(*a*) (*b*) (*c*)

Fig. 7. Transmission topography of 250 μm thick silicon crystal implanted with 60 keV phosphorus ions through a 10 × 10 mm hole. Dose = 10^{13} ion cm^{-2}. (*a*) Crystal tilted 2′, diffracted beam. (*b*) Crystal tilted 2′, transmitted beam. (*c*) Crystal tilted 0·8′, diffracted beam.

For higher ion concentrations the fringe pattern changes radically owing to the increased strains in the crystal. Now the *Pendellösung* fringes are seen even for $\beta = 0$ because of the greater curvature of the crystal. Fig. 8 shows such topographs for an ion dose of $1{\cdot}1 \times 10^{15}$ ion cm^{-2} implanted through a 6 mm circular hole. The fringes now become straight vertical lines inside the implanted region. The pattern is equal to that of Fig. 6 except for a 90° rotation. This indicates that the strain field in this region is homogeneous. In this case the fringe pattern inside the implanted area is practically independent of β, and again the distance between the fringes, as measured along a horizontal line, is a direct measure of the curvature and hence also of the strain in the crystal. Outside the implanted spot where the strain field is weaker it can be separated into horizontal and vertical components by measuring the vertical and horizontal distances between the fringes. Two topographs are shown for different Bragg angles, $\eta = 0{\cdot}35$ in Fig. 8(*a*) and $\eta = -1$ in Fig. 8(*b*).

The *Pendellösung* pattern is rather similar to the moiré pattern obtainable by the interferometer method (Bonse & Hart, 1965; Gerward, 1973) and the possibility of examining strain fields is by and large the same for the two methods. However, as compared to the interferometer method the technique described here has the advantage of a much simpler sample preparation.

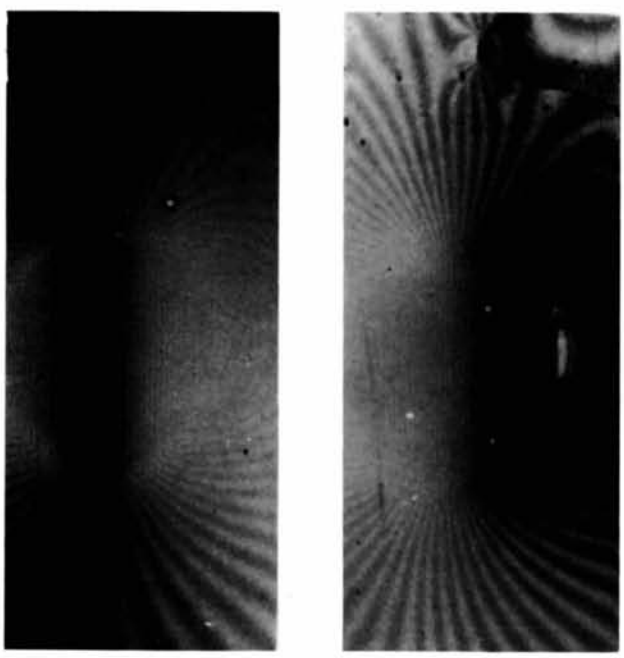

(*a*) (*b*)

Fig. 8. Transmission topography of 250 μm thick silicon crystal implanted with 60 keV phosphorus ions through a 6 mm hole. Dose = $1{\cdot}1 \times 10^{15}$ ion cm^{-2}. (*a*) Crystal rotated, $\Delta\theta \simeq 0{\cdot}5''$. (*b*) Crystal rotated, $\Delta\theta \simeq -1{\cdot}3''$.

It may be noted for instance that the *Pendellösung* pattern depends on the strain field in quite a different way from that of the interferometer. Variations in the lattice constant and in the angle of the diffracting planes are directly separable in the moiré pattern, whereas they influence the *Pendellösung* pattern in a similar way. However, as variations in the lattice constant are insensitive to the sign of the Bragg angle, the two effects may be separated by comparing 220 and $\bar{2}\bar{2}0$ reflections. A more detailed analysis of the strain field will be given later.

Conclusions

It has been shown that by using an X-ray beam collimated by two asymmetrically cut crystals plane-wave fields are obtained which may interfere in such a manner that *Pendellösung* effects are observed. The positions of the peaks in the experimental rocking curves are in good agreement with the positions calculated using the dynamical theory of diffraction for plane X-ray waves. The peaks are significant for crystal thicknesses up to more than 1 mm for practically unpolarized X-rays. The topographical method described has been used for visualizing strains in samples implanted with 60 keV phosphorus ions. Weak strain fields may be determined as deviations from a horizontal fringe pattern when the crystal is tilted, and the sensitivity may be adjusted through the tilting angle. Strain fields may be determined for ion doses down to 10^{12} ion cm^{-2}.

The author wishes to thank O. Pedersen for technical assistance and G. Christiansen for the computational work. He is also indebted to Topsil A/S for supplying the silicon crystals. Financial support by the Danish Natural Science Research Council is greatly appreciated.

References

Batterman, B. W. & Cole, H. (1964). *Rev. Mod. Phys.* **36**, 681–717.
Bonse, U. & Hart, M. (1965). *Z. Phys.* **188**, 154–164.
Gerward, L. (1973). *Z. Phys.* **259**, 313–322.
Hart, M. & Lang, A. R. (1965). *Acta Cryst.* **19**, 73–77.
Kato, N. (1961). *Acta Cryst.* **14**, 526–532, 627–636.
Kato, N. & Lang, A. R. (1959). *Acta Cryst.* **12**, 787–794.
Kikuta, S. & Kohra, K. (1970). *J. Phys. Soc. Jpn*, **29**, 1322–1328.
Kohra, K. & Kikuta, S. (1968). *Acta Cryst.* A**24**, 200–205.
Lefeld-Sosnowska, M. & Malgrange, C. (1968). *Phys. Status Solidi*, **30**, K 23–25.
Malgrange, C. & Authier, A. (1965). *C.R. Acad. Sci.* **261**, 3774–3777.
Renninger, M. (1963). *Crystallography and Crystal Perfection*, Edited by G. N. Ramachandran, pp. 145–151. London: Academic Press.